Check for updates

View metadata, citation and similar papers at core.ac.uk

View Article Online

brought to you by CORE

provided by Repositorio Universidad de Zaragoza

Dalton Transactions

Accepted Manuscript

This article can be cited before page numbers have been issued, to do this please use: E. Bartolomé, A. Arauzo, J. Luzón, S. Melnic, S. Sova, D. Prodius, J. Bartolomé, A. Amann, M. Nallaiyan and S. Spagna, *Dalton Trans.*, 2019, DOI: 10.1039/C8DT05044A.

This is an Accepted Manuscript, which has been through the Royal Society of Chemistry peer review process and has been accepted for publication.

Accepted Manuscripts are published online shortly after acceptance, before technical editing, formatting and proof reading. Using this free service, authors can make their results available to the community, in citable form, before we publish the edited article. We will replace this Accepted Manuscript with the edited and formatted Advance Article as soon as it is available.

You can find more information about Accepted Manuscripts in the author guidelines.

Please note that technical editing may introduce minor changes to the text and/or graphics, which may alter content. The journal's standard Terms & Conditions and the ethical guidelines, outlined in our author and reviewer resource centre, still apply. In no event shall the Royal Society of Chemistry be held responsible for any errors or omissions in this Accepted Manuscript or any consequences arising from the use of any information it contains.

ROYAL SOCIETY OF CHEMISTRY

rsc.li/dalton

Dalton Transactions

View Article Online
DOI: 10.1039/C8DT05044A

Slow relaxation in $\{Tb_2Ba(\alpha\text{-fur})_8\}_n$ polymer with Ln=Tb(III) non-Kramers ion

Received 00th January 20xx,
Accepted 00th January 20xx

DOI: 10.1039/x0xx00000x

www.rsc.org/

E. Bartolomé[a], A. Arauzo[b,c], J. Luzón[c,f], S. Melnic[d], S. Shova[e], D. Prodius[d, §], J. Bartolomé[b], A. Amann[e], M. Nallaiyan[e], S. Spagna[e]

We report the synthesis, crystal structure and magnetic properties of a new heteronuclear polymeric complex based on non-Kramers Tb ion and carboxylic α-fur= C_4H_3OCOO ligands: $\{[Tb_2Ba(\alpha\text{-fur})_8(H_2O)_4]\cdot 2H_2O\}_n$. The α-furoate ligands consolidate 1D zig-zag chains running along the c-axis, formed by Tb_2 dimers separated by Ba ions. *Ab initio* calculations, in combination with the fit of experimental data, predict that the single-ion magnetic ground state is highly anisotropic (g_z*=17.8) and consists of a quasi-doublet with Δ_{Tb}/K_B=3.22 K gap, well separated from the next excited state, while the gap for the Tb_2 dimer is Δ_{2Tb}/K_B=2.58 K. Static magnetization and heat capacity measurements show that, magnetically, the system can be modeled as dimers of non-Kramers Tb ions, coupled by an antiferromagnetic intradimer interaction J'^*/k_B =-1.6 K. Dipolar interactions couple the Tb ions in the dimer with their first neighbour ions along the chain, with J''^*/k_B =-0.15 K, and with the surrounding ions out of the chain, with maximum J'''^*/k_B =-0.03 K. Ac susceptibility measurements in H=0 performed down to 50 mK temperatures have enabled us to observe slow relaxation of the magnetization, with an Orbach-like activation energy of U/k_B=1.1 K. It is assigned to sluggish response of the 3D spin system due to a short-range ordering, possibly enhanced by the presence of disorder caused by defects in the polymeric chains. Under the application of a magnetic field, the system slowly relaxes by two distinct direct processes, strongly affected by a phonon bottleneck effect. We discuss the different relaxational phenomenology of the new complex in comparison with that of the isostructural $\{[Dy_2Ba(\alpha\text{-fur})_8(H_2O)_4]\cdot 2H_2O\}_n$, differing only in the Kramers nature of the ion, and the mononuclear $\{Ln(\alpha\text{-fur})_3(H_2O)_3\}_n$ (Ln=Tb, Dy) complexes, previously reported.

1. Introduction

Lanthanide-based Molecular Magnets have received an increasing level of attention in the past years[1,2,3] due to their interesting properties and foreseeable application in information storage, quantum-computing, switching etc. The slow-relaxation dynamics of such low-dimensional magnets relies upon the formation of an energy barrier (U_{eff}) between two stable energy states. In single-ion magnets (SIMs), U_{eff} depends basically on the molecule's anisotropy, given by the type of lanthanide[4,5] used and its coordination environment: its symmetry[6,7], number and type of coordinating atoms[8,9], ligands in the first and even the second coordination sphere[10,11]. Extremely large activation energies at record blocking temperatures have been recently reported for certain Dy metallocenes thanks to the rigid, axial geometry achieved by the ligands, $[Dy(Cp^{ttt})_2](U_{eff}$ =1760 K at T_B=60 K)[3,12] and $[(Cp^{iPr5})Dy(Cp^*)]^+$ (U_{eff} =2217.2K at T_B=80 K)[13], the later result paving the way for the development of nanomagnet devices at practical, liquid-nitrogen temperatures.

For lanthanide single-molecule magnets (SMMs), magnetic relaxation is also essentially dominated by single-ion anisotropy, at least within the SQUID's range of temperatures T>1.8 K where most complexes are characterized, given the weakness of 4f-4f interactions. However, by decreasing sufficiently the temperature intra- and inter-molecular interactions become competitive. Thus a crossover from SIM relaxation of the individual ions to SMM behavior upon cooling can occur, as observed in some dimeric Ln_2 compounds[14,15]. Besides, the effect of Kramers and non-Kramers rare earth substitutions on the SMM behavior of transition metal – rare earth complexes have been investigated[16,17].

$[Tb_2]$ compounds have attracted interest for different reasons. On one hand, they have been proposed as candidates for the realization of quantum gates, using asymmetric, weakly-coupled [TbTb'] compounds to perform CNOT and SWAP operations between two coupled two-level bits (*qubits*)[18,19], or the implementation of multi-level quantum bits (*qudits*)[20] using $[Tb_2Pc^{Hx8}Pc_2]$. Besides, Tb_2Pc_3 (double-decker phthalocyanines) have been intensively investigated owing to their tendency toward high energetic barriers[21] and potential customization onto surfaces. Recently, a SMM formed by two $[TbPc_2]^0$ units connected via fused-phthalocyanine ligand with a large U_{eff}=847 K at ca. T_B=16 K has been reported, assigned to the D_{4d} geometry and weak inter- and intramolecular interactions, acting like a bias H_{bias}, reducing quantum tunneling.[22]

[a] Escola Universitària Salesiana de Sarrià (EUSS), Passeig Sant Joan Bosco 74, 08017-Barcelona, Spain.
[b] Servicio de Medidas Físicas. Universidad de Zaragoza, Pedro Cerbuna 12, 50009 Zaragoza, Spain.
[c] Instituto de Ciencia de Materiales de Aragón, CSIC-Universidad de Zaragoza, Pedro Cerbuna 12, 50009 Zaragoza, Spain.
[d] Institute of Chemistry, Academy of Sciences of Moldova, Academiei 3, MD-2028,Chisinau, Moldova.
[e] "Petru Poni" Institute of Macromolecular Chemistry, Alea Gr. Ghica Voda 41A, 700487 Iasi, Romania
[f] Centro Universitario de la Defensa. Academia General Militar, Zaragoza, Spain.
[g] Quantum Design Inc.,San Diego,CA92121, USA
[§] Current address: Ames Laboratory, US Department of Energy and Critical Materials Institute, Ames, IA-50011-3020, USA

Electronic Supplementary Information (ESI) available: [S1. 3D crystal structure of the $\{Tb_2Ba\}$ compound, S2. Ab initio calculation results, S3. Heat capacity measurements, S4. Susceptibility modelization, S5. Magnetic relaxation results]. See DOI: 10.1039/x0xx00000x

Published on 20 March 2019. Downloaded by University of Edinburgh on 3/25/2019 10:48:02 AM.

Dalton Transactions Accepted Manuscript

Please do not adjust margins

View Article Online DOI: 10.1039/C9DT00444A

Published on 20 March 2019. Downloaded by University of Edinburgh on 3/25/2019 10:48:02 AM.

Dalton Transactions Accepted Manuscript

One-dimensional (1D) lanthanide-based complexes represent ideal model systems to investigate how relaxation behavior depends on the relative strength between single-ion's anisotropy *vs.* Ln-Ln interactions. In polymeric systems with negligible interactions slow relaxation is caused by SIM behavior of the constituents[23–31], as can be proven by magnetic dilution experiments[32]. On the other hand, collective single-chain magnet (SCM) behavior has been reported in many 1D systems with strong ferromagnetic intrachain interactions[33], but also in a few antiferromagnetic (AF) chains, allowed either by AF canting of spins[34] or by the existence of defects breaking the chain in segments with odd and even number of ions[35].

In the past few years, our group has applied a multi-technique characterization of polymeric Ln-furoate complexes down to mK temperatures to investigate relaxational behavior as intrachain and interchain interactions become progressively competitive. The furoate ligand α-fur=C_4H_3OCOO, acting in bridging mode, has demonstrated to be efficient in consolidating stable 1D chains containing lanthanides[36]. Using this ligand, we were able to synthesize and characterize a whole family of furoate complexes, including homonuclear $\{Ln(\alpha\text{-fur})_3\}_n$, with both Kramers (Ln = Dy[32]) and non-Kramer ions (Ln = Tb[35]); heteronuclear $\{[Dy_2Sr(\alpha\text{-fur})_8(H_2O)_4]\}_n{\cdot}2H_2O$[37], $\{[Dy_2Ba(\alpha\text{-fur})_8(H_2O)_4]{\cdot}2H_2O\}_n$[38] and luminescent mixed $\{Tb_xEu_{1-x}(\alpha\text{-fur})_3\}_n$[39] complexes.

Substantial differences in the relaxational behavior were observed between isostructural compounds $\{Dy(\alpha\text{-fur})_3(H_2O)_3\}_n$ **(Dy)** and $\{Tb(\alpha\text{-fur})_3(H_2O)_3\}_n$ **(Tb)**, differing only in the Kramers or non-Kramers nature of the ion, and also between mononuclear $\{Dy(\alpha\text{-fur})_3(H_2O)_3\}_n$ **(Dy)** and $\{[Dy_2Ba(\alpha\text{-fur})_8(H_2O)_4]{\cdot}2H_2O\}_n$[38] **($Dy_2Ba$)**. To complete this systematic study, we report here the synthesis and magneto-structural characterization of the 1D α-furoate compound, $\{[Tb_2Ba(\alpha\text{-fur})_8(H_2O)_4]{\cdot}2H_2O\}_n$, **($Tb_2Ba$),** with non-Kramers Tb ion. This compound is isostructural to the Dy substitution. It is formed by trinuclear (Tb-Ba-Tb) clusters, linked to adjacent molecules via furoic bridges, forming zig-zag chains. The end-to-end binding of the adjacent Tb-Ba-Tb clusters result in the formation of magnetically coupled Tb-Tb dimers, which are the object of study of the present paper. The relaxational phenomenology of this new complex compared with the above referred α-furoates is discussed. Our work describes a rare example of AF coupled dimers of non-Kramers in a polymeric chain displaying slow relaxation dynamics.

2. Experimental

A general protocol described in Ref.[40] was applied for the preparation of the metal complex $\{[Tb_2Ba(\alpha\text{-}C_4H_3OCOO)_8(H_2O)_4]{\cdot}2H_2O\}_n$ **(Tb_2Ba)**, abbreviated $\{Tb_2Ba(\alpha\text{-fur})_8\}$, as follows: solutions of $Ba(C_4H_3OCOO)_2{\cdot}4H_2O$ (0.30 g, 0.70 mmol) in 5 ml of water and $Tb(ClO_4)_3{\cdot}6H_2O$ (0.39 g, 0.70 mmol) in 10 ml of ethanol were stirred until formation of white gel-mass. 10 ml of water were added to the obtained compound which was stirred for a further period of 20 minutes at 50°C to afford a clear solution. After a week a white microcrystalline product was filtered off, quickly washed with water and air-dried. IR (KBr): ν/cm^{-1}: 3500b, 1627m, 1586vs, 1221m, 1202s, 1136w, 1072s, 1007s, 933m, 883m, 761s, 753w, 611w, 598m, 460s. Calc. for $C_{40}H_{36}O_{30}Tb_2Ba$: C, 33.06; H, 2.48; Found: C, 33.10; H, 2.51.

X-ray diffraction measurements were carried out with an Oxford-Diffraction XCALIBUR E CCD diffractometer equipped with graphite-monochromated Mo-K_α radiation. The crystals were placed 40 mm from the CCD detector and 233 frames were measured each for 15 s over 1° scan width. The unit cell determination and data integration were carried out using the CrysAlis package of Oxford Diffraction[41]. The structure was solved by direct methods using Olex2[42] software with the SHELXS[43] structure solution program and refined by full-matrix least-squares based on and refined by full-matrix least-squares on F^2 with SHELXL-97[43] using an anisotropic model for non-hydrogen, atoms. All H atoms attached to carbon were introduced in idealized positions (d_{CH} = 0.96 Å) using the riding model with their isotropic displacement parameters fixed at 120% of their riding atom. Positional parameters of the H attached to O atoms were obtained from difference Fourier syntheses and verified by the geometric parameters of the corresponding hydrogen bonds. The main crystallographic data together with refinement details are summarized in Table 1. Selected bond distances are listed in Table S1. CCDC-1890684 contains the supplementary crystallographic data for this contribution. These data can be obtained free of charge via www.ccdc.cam.ac.uk/conts/retrieving.html (or from the Cambridge Crystallographic Data Centre, 12 Union Road, Cambridge CB2 1EZ, UK; fax: (+44) 1223-336-033; or deposit@ccdc.ca.ac.uk).

The magnetization, dc and ac susceptibility of powdered samples were measured, above 1.8 K, using a Quantum Design superconducting quantum interference device (SQUID) magnetometer. Ac measurements were done at an excitation field of 4 Oe, and under dc fields between 0-10 kOe, while sweeping the frequency between 0.1 and 1000 Hz. Measurements on powdered

Table 1. Crystallographic data, details of data collection and structure refinement parameters for **(Tb_2Ba)**.

Complex	$\{[Tb_2Ba(\alpha\text{-fur})_8(H_2O)_4]{\cdot}2H_2O\}_n$
CCDC	1890684
Empirical formula	$C_{40}H_{36}BaO_{30}Tb_2$
Formula weight	1451.87
Temperature/K	160.00(10)
Crystal system	monoclinic
Space group	$P2_1/c$
a/Å	11.2953(5)
b/Å	22.4294(7)
c/Å	10.5545(4)
α/°	90.00
β/°	116.025(5)
γ/°	90.00
V/Å^3	2402.81(16)
Z	2
D_{calc}/mg/mm^3	2.007
μ/mm^{-1}	3.821
Crystal size/mm^3	0.5 × 0.03 × 0.03
ϑ_{min}, ϑ_{max}(°)	4.02 to 50.04
Reflections collected	10344
Independent reflections	4245 [R_{int} = 0.0339, R_{sigma} = 0.0483]
Data/restraints/parameters	4245/0/331
GOF[c]	1.068
R_1[a]($I>2\sigma(I)$)	R_1 = 0.0302, wR_2 = 0.0532
wR_2[b](all data)	R_1 = 0.0379, wR_2 = 0.0564
Largest diff. peak/hole/e Å^{-3}	1.06/-0.84

[a] $R_1 = \Sigma||F_o| - |F_c||/\Sigma|F_o|$, [b] $wR_2 = \{\Sigma[w\,(F_o^2 - F_c^2)^2]\,/\Sigma[w(F_o^2)^2]\}^{1/2}$.
[c] GOF = $\{\Sigma[w(F_o^2 - F_c^2)^2]\,/(n-p)\}^{1/2}$, where *n* is the number of reflections and *p* is the total number of parameters refined

This journal is © The Royal Society of Chemistry 20xx

View Article Online
DOI: 10.1039/C8DT05044A

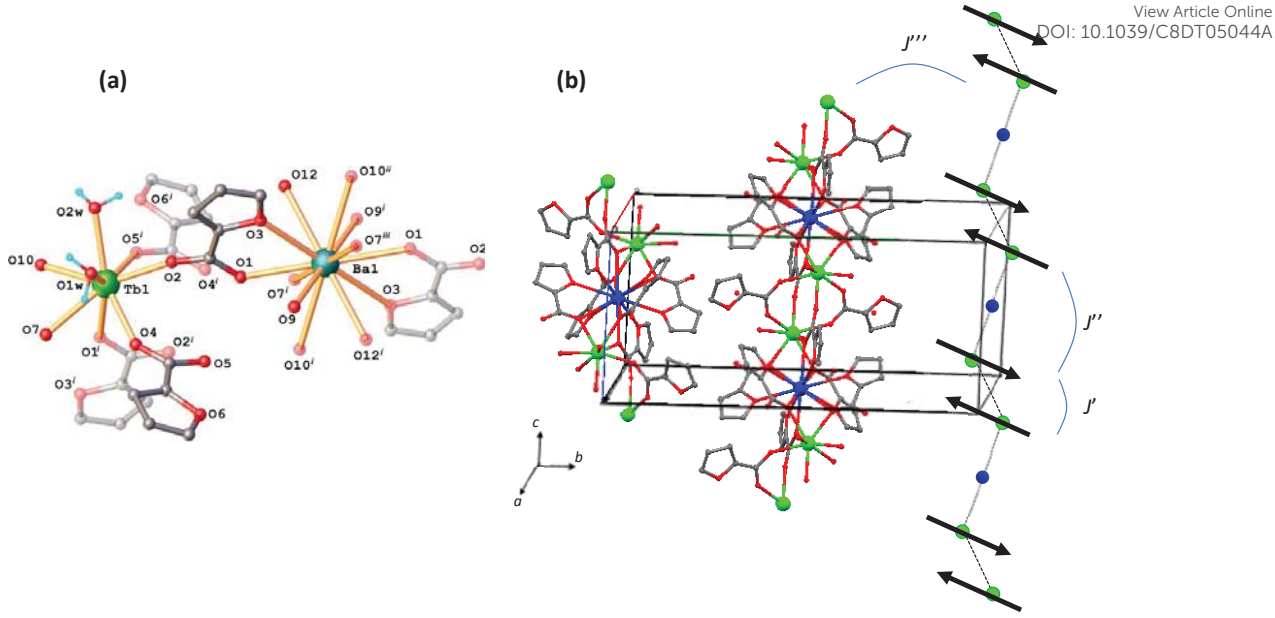

Fig. 1 (a) Extended asymmetric unit in **(Tb_2Ba)** with atoms obtained by symmetry-transformations shown semi-transparent. Symmetry codes: [i]1 –x, 1 – y, [ii]1 – z; x, y, z -1; [iii]1 –x, 1 – y, –z.; (b) Schematics showing the assembly of zig-zag chains along the *c*-axis, and EAM and interactions between the induced magnetic moments, as calculated by *ab initio*.

samples were performed adding Daphne oil to fix the grains at low temperatures.

Ac susceptibility measurements in the very low temperature range (50 mK - 3.0 K) under zero applied field were performed using the recently developed AC susceptometer by Quantum Design housed in the dilution refrigerator (DR) option for a PPMS[44]. The amplitude of the excitation field was H_a=0.5 Oe, and the frequency range 10 Hz< f <10 kHz. A 3 mm diameter powder pressed pellet was mounted on a sapphire rod attached to the DR sample stage.

Heat capacity $C(T)$ under different applied fields (0-30 kOe) was measured on a powder pressed pellet fixed with Apiezon N grease, using a Quantum Design Physical Properties Measurement System (PPMS).

3. Structural characterization

Single-crystal X-ray study reveals that **(Tb_2Ba)** crystallizes in the space group $P2_1/c$ of monoclinic system, and is formed by Tb-Ba-Tb trinuclear clusters linked end-to-end. The Tb^{3+} and Ba^{2+} ions within the cluster, and the Tb^{3+} - Tb^{3+} ions of adjacent are linked due to the bridging function of the polydentate furoic acid ligands to form a 1D coordination polymer $\{[Tb_2Ba\text{-}(\alpha\text{-}C_4H_3OCOO)_8(H_2O)_4]\cdot 2H_2O\}_n$ as depicted in Figure 1b. The shortest Tb···Tb and Ba…Tb separations within the infinite chain are equal to 4.4499(4) Å and 4.0743(3) Å, respectively. The coordination number of Tb1 atom is equal to 8, the Tb1–O bond distances being in the range between 2.306(3) and 2.526(3) Å (see Table S1).

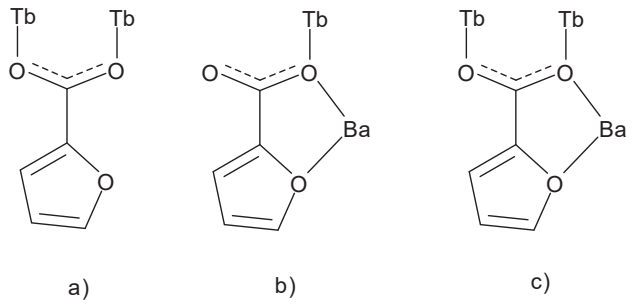

Fig. 2 Scheme showing the three different M-M' coordination modes in the complex.

The coordination environment of the Tb atom is completed by the oxygen atoms originating from carboxyl groups and water molecules (Fig. 1a). Its coordination polyhedron can be characterized as a distorted square-antiprism (SAP). The polyhedron of the Ba atom, which occupies the special position on the inversion centre, can be characterized as a slightly distorted icosahedron[38] formed by twelve oxygen atoms. The coordination core of the Ba atoms is formed by the oxygen atoms of carboxylic groups as well as by the oxygen atoms of the heterocycles: each of the six carboxylate ligands binds to a Ba ion through the one oxygen atom of the furoic rings, and one oxygen atom of the carboxylic groups.

There are four moieties of 2-furan-carboxylic acid with deprotonated carboxylic groups in the independent unit cell. It should be mentioned that they exhibit a different structural function in the crystal, as it is shown in Fig. 2. One of the ligands is coordinated through the carboxylate group (O4 and O5) in bidentate-bridging fashion. In this case, the heterocyclic oxygen atom (O6) is not involved into coordination to metal (Fig. 2a). Two 2-furan-carboxylic moieties exhibit the same coordination mode where the carboxylate oxygen (O7' or O10') fulfills the bridging function between Ba and Tb atoms, while the heterocyclic oxygen (O9 or O12) is monocoordinated to the Ba atom (Fig. 2b). The third type of the furan-carboxylic moiety is a tetradentate bridging ligand being coordinated to two Tb through the carboxylate group (O1 and O2) and one Ba atoms through carboxylate oxygen (O1) as well as heterocyclic oxygen (O3) (Fig. 2c).

Thus, in the present structure there are three coordination modes: bidentate bridging (Fig. 2a), through carboxyl groups of the ligand, tridentate chelating-bridging, with the formation of a

Published on 20 March 2019. Downloaded by University of Edinburgh on 3/25/2019 10:48:02 AM.

Dalton Transactions Accepted Manuscript

View Article Online
DOI: 10.1039/C8DT05044A

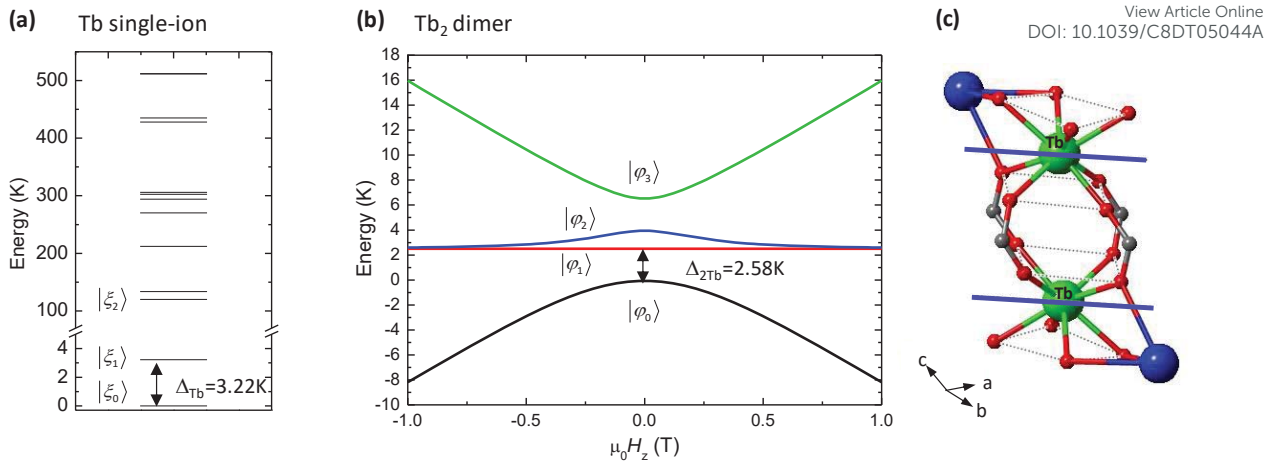

Fig. 3 Results of *ab initio* calculations: (a) energy levels for each Tb(III), with $\Delta_{Tb} / k_B = 3.22$ K , and (b) energy level diagram for the Tb_2 dimer, with intradimer interaction $J'^{*} / k_B = -1.6$ K , as a function of a magnetic field applied along a z-axis along parallel to the EAM; (c) Schematics showing the transversal direction of the EAM of each Tb ion with respect to the C_4-axis of its distorted SAP coordination polyhedron.

monoatomic carboxyl bridge M-O-M (Fig. 2b), and tetradentate, which is a superposition of the two previous ones (Fig. 2c).

In the crystal, the polymeric coordination chains are assembled through the system of O-H…O hydrogen bonding involving the coordinated and solvate water molecules to form a three-dimensional supramolecular network, as shown in Fig. S1.

4. *Ab initio* and theory

Relativistic *ab initio* calculations were performed in order to determine the energy level structure of the Tb(III) multiplet ground state and the main axes of the effective gyromagnetic *g**-tensor, in an effective spin S*=1/2 model, for the two lowest states, using the CASPT2/RASSI-SO[45] method as implemented in the MOLCAS 8.2 package[46]. *Ab initio* calculations were performed on a molecular cluster in which the atomic positions were extracted from the x-ray crystal structure. The cluster model includes the studied Tb ion, an Y(III) ion in the position of the other Tb ion of the dimer and the two closest Ba ions. The model also includes the furoic ligands and water molecules surrounding the studied Tb ion. The orientation of these water molecules can drastically influence the magnetic anisotropy of the lanthanide ion[47]. However, the x-ray technique does not allow to accurately determining the position of the hydrogen atoms. Therefore, in this compound we have placed the hydrogen atoms of the two Tb-coordinated water molecules in order to form H-bonds with near oxygen atoms. In order to reduce the computation time, without a significant loss of accuracy, the other ligands around the second Tb ion and the two Ba ions are adequately replaced by either OH- groups or water molecules. The replacement of the second Tb ion by an Y ion is in order to reduce the active space.

All atoms were represented by basis sets of atomic natural orbitals from the ANO RCC library[45]. The following contractions were used: [9s8p6d4f2g1h] for the Tb ion; [4s3p1p] for the O and C atoms in the three first shells around the Tb ion; [3s2p] for the rest of the O and C atoms, [7s6p4d] for the Ba ion, [7s6p4d2f] for the La ion and [2s] for the H- atoms. Finally, the chosen CASSCF active space consisted of the Tb 4f orbitals, containing eight electrons in seven orbitals [CASSCF(8,7)].

The *ab initio* electronic energy level structure of the $^7F_6$ Tb(III) ground multiplet is represented in Figure 3a. Using the easy axis of magnetization (EAM) as the quantization axis, the composition of the corresponding 13 states , $\{|\xi_i\rangle\}$, in terms of the J_z eigenstates is summarized in Table S2. The ground $|\xi_0\rangle$ and the first excited $|\xi_1\rangle$ states are mainly an equally weighted mixture of the $|6,-6\rangle$ and the $|6,+6\rangle$ J_z eigenstates, with some small contribution of the $|6,\pm4\rangle$ and $|6,\pm4\rangle$ states. Both lowest energy states are separated by a small energy gap of Δ_{Tb}/k_B =1.13 K (a value that will be revised latter in this work, see below), while the second excited state $|\xi_2\rangle$ is well above, at an energy ~120 K. For the quasi-doublet ground state (GS), the *ab initio* gyromagnetic factors along the main single-ion anisotropy axes are $g_x^*=g_y^*=0$, in agreement with the Griffith's theorem[48] for non-Kramers ions, and $g_z^*=17.54$ (in $S^*=1/2$ Hamiltonian). The large value of g_z^*, due to the large contribution of the $|6,\pm6\rangle$ states in the composition of the GS doublet, indicates a large uniaxial magnetic anisotropy. The obtained $g_z^*=17.54$ is actually the signature of a small deviation of g_J from ideal g_J =1.5 value and/or a slight "impurity" of the J_z, deviating from ideal J_z={-6, +6}.

Since the two Tb ions of the Tb_2Ba unit occupy equivalent symmetry sites, their EAM are parallel to each other. As shown in Figure 3c, the EAM of each Tb ion is transversal to the quasi-C_4 symmetry axis of its distorted SAP coordination sphere. The EAM of Tb ions is nearly perpendicular (89.1º) to the direction of the polymeric chain (Figure 1b). It is worth noting that, in the absence of interactions and under *H*=0, the calculated magnetic moment of the two lowest states of the Tb ion is zero, $\langle \xi_i | g_J \mu_B J_z | \xi_i \rangle = 0$, given the composition of both states (see Table S2).

The *ab initio* determination of the orientation of the easy axes of magnetization for the Tb ions in the crystallographic cell also allowed us to estimate the dipolar interaction between the magnetic

	d(Å)	$J^*_{dip}(K)$	$J^*(K)$
Intradimer J'/k_B	4.487	-1.02	-1.6
Interdimer J''/k_B	8.161	-0.15	-0.1
Interchain J'''/k_B	7.994	-0.03	-

Table 2. Summary of intradimer, inter-dimer and inter-chain interactions expressed in terms of the $S^*=1/2$ model, i) of the dipolar type obtained from *ab initio* calculations, and ii) total (dipolar+exchange) interaction experimentally obtained.

Published on 20 March 2019. Downloaded by University of Edinburgh on 3/25/2019 10:48:02 AM.

Dalton Transactions Accepted Manuscript

This journal is © The Royal Society of Chemistry 20xx

View Article Online
DOI: 10.1039/C9DT00...

moments of two Tb ions. This dipolar interaction is given by the following Hamiltonian:

$$H_{dip} = -\frac{\mu_0}{4\pi r^3}\left(3(\vec{m}_1\cdot\hat{r})(\vec{m}_2\cdot\hat{r}) - \vec{m}_1\vec{m}_2\right). \quad [1]$$

This Hamiltonian is very anisotropic, and depends not only on the relative orientation of the magnetic moments but also on the $\vec{r}$ vector connecting them. However, in our case, where all the EAM are parallel and where, due to the large single-ion magnetic anisotropy, the magnetic moment can be approximated to $g_J\mu_B J_z$, the dipolar Hamiltonian can be rewritten as:

$$H_{dip} = -\frac{\mu_0 g_J^2 \mu_B^2}{4\pi r^3}\left(3\cos^2\theta - 1\right)J_{1z}J_{2z}. \quad [2]$$

Considering only the two lowest states of the Tb ions, this Hamiltonian can be mapped in terms of a S*=1/2 model $(-2J^*\vec{S}_1^*\cdot\vec{S}_2^*)$ with:

$$J_{dip}^* = \frac{\mu_0 g_z^{*2}\mu_B^2}{8\pi r^3}\left(3\cos^2\theta - 1\right). \quad [3]$$

Using this expression, the three strongest dipolar interactions are listed in Table 2. It can be observed that the intradimer dipolar interaction, J_{dip}'*/k_B=-1.02 K, is one order of magnitude larger than the dipolar interdimer interaction along the chain, J_{dip}"*/k_B=-0.15 K, which in turn is almost one order of magnitude larger than any other dipolar interaction.

Taking into account the relative strength of the previous dipolar interactions and that super-exchange magnetic interaction will be negligible outside the Tb-Tb dimer, the magnetism of the compound could be modeled, in first approximation, by a Tb-Tb dimer system. Therefore, the results of the *ab initio* calculations have been employed for fitting the experimental data reported in the next sections by means of a dimer Hamiltonian considering two identical Tb(III) ions:

$$H_{\text{dimer}} = \sum_{i=1,2} H_{Tb,i} - 2J'\vec{J}_1\cdot\vec{J}_2 + \sum_{i=1,2} g_J\mu_B\vec{J}_i\cdot\vec{H} + H_{hyp}, \quad [4a]$$

$$H_{hyp} = \sum_{i=1,2}\left(A\,\vec{J}_i\cdot\vec{I}_i - g_N\mu_B\vec{I}_i\cdot\vec{H}\right), \quad [4b]$$

where $H_{Tb,i}$ is the electronic single-ion Hamiltonian producing the single-ion eigenstates and their corresponding energies, the second Hamiltonian term accounts for the intradimer magnetic interaction, and the third one is the Zeeman term. At low temperatures below 1 K spin-nuclear interactions play a role in the magnetic behavior. Indeed, Tb(III) has a nuclear spin of I = 3/2, with a 100% natural abundance, yielding (2I + 1) = 4 substates with nuclear spin projections M_I=-3/2, -1/2, 1/2, 3/2. To take account of this interaction, the dimer Hamiltonian includes the term H_{hyp}, Eq. [4b], where the first term corresponds to the electron-nuclear hyperfine interaction, and the second is the nuclear Zeeman term with g_N=1.342. The dimer Hamiltonian in the S*=1/2 approximation is given in S.I, Eq. [S4].

Figure 3b shows the four lowest electronic energy levels for the Tb_2 dimer, and its dependence with a magnetic field applied along the EAM axis. The pseudo-doublet ground states of the two interacting Tb(III) ions lead to four energy states at 0.00 K, 2.58 K, 4.02 K and 6.60 K. The dimer eigenfunctions, $\{|\varphi_i\rangle\}$, diagonalizing H_{dimer} (with $H_{hyp}\approx 0$) can be written as lineal combinations of the single-ion functions, $|\varphi_i\rangle = \sum_{jk} C_{jk}^i |\xi_j\rangle|\xi_k\rangle$. In particular, the four lowest states of the dimer can be decomposed in terms of the two lowest single-ion eigenfunctions as:

$$\begin{aligned}
|\varphi_3\rangle &= 0.99|\xi_1\rangle|\xi_1\rangle + 0.11e^{0.23\pi i}|\xi_0\rangle|\xi_0\rangle \\
|\varphi_2\rangle &= \left(|\xi_1\rangle|\xi_0\rangle + |\xi_0\rangle|\xi_1\rangle\right)/\sqrt{2} \\
|\varphi_1\rangle &= \left(|\xi_0\rangle|\xi_1\rangle - |\xi_1\rangle|\xi_0\rangle\right)/\sqrt{2} \\
|\varphi_0\rangle &= 0.99|\xi_0\rangle|\xi_0\rangle - 0.11e^{0.23\pi i}|\xi_1\rangle|\xi_1\rangle
\end{aligned} \quad [5]$$

where only products with a weight larger than 1% have been considered. The magnetic interaction has two main effects: first, producing a slight admixture of the $|\xi_0\rangle|\xi_0\rangle$ and the $|\xi_1\rangle|\xi_1\rangle$ products for the dimer ground $|\varphi_0\rangle$ and third excited $|\varphi_3\rangle$ states, and second, combining the $|\xi_0\rangle|\xi_1\rangle$ and the $|\xi_1\rangle|\xi_0\rangle$ products in an antisymmetric or symmetric function for, respectively, the $|\varphi_1\rangle$ and $|\varphi_2\rangle$ excited states, breaking their degeneracy by creating an energy gap of ca. 1.44 K between both states, as can be observed in Figure 3b.

A consequence of the stronger effect of the single-ion crystal field with respect to the magnetic interaction is that the dimer states cannot be labeled as pure ferro or antiferro states. This can be clearly observed by decomposing the dimer states in products of the J_z eigenstates of the two single-ions, $\{|6,M\rangle|6,M'\rangle\}$, see Table S5. In particular, despite the antiferromagnetic interaction, the ground state is not an AF state. In fact only the first excited state has a clear AF character, $|\varphi_1\rangle = 0.64(|6,6\rangle|6,-6\rangle - |6,-6\rangle|6,6\rangle)$, as can be also inferred from Figure 3b, showing that its energy does not change with the applied magnetic field.

It is worth to remark that within this dimer model, neglecting all other interactions, the expected magnetic moment of the Tb_2 dimer at H=0 would be quenched, $\langle\varphi_i|g_J\mu_B J_z|\varphi_i\rangle = 0$ (as can be deduced as well from the zero slope of the energy levels at H=0 in Figure 3b). Nevertheless, further weak but abundant interdimer and interchain dipolar interactions, acting like an internal field, would induce non-zero magnetic moments. The effect of these dipolar interactions is expected to be more important at very low temperatures, and is plausibly at the origin of the excess $\chi'(T)$ compared to the theoretical prediction observed at mK, as will be discussed in Section 5.

At temperatures below 1 K, the hyperfine contribution is non negligible (as it becomes apparent from the heat capacity measurements, *vide infra*). The H_{dimer} Hamiltonian, including the H_{hyp}, operates on the set of wavefunctions, product of the monoatomic electronic for J=6 times the nuclear for I=3/2, $|\xi_i, I_z\rangle = |\xi_i\rangle|I, I_z\rangle$, This base has 52 elements. The dimeric total wavefunctions are generated as the product $|\phi_k\rangle = |\xi_{i,1}, I_{z.1}\rangle|\xi_{ij,2}, I_{z.2}\rangle$, forming a base of 2704 elements. To reduce computation time, for the calculation of the observables, a restricted electronic-nuclear base of the above, considering only the two lowest energy monoatomic electronic eigenfunctions (i=0,1), was used.

The dimeric model was used to calculate the susceptibility $\chi(T)$, the magnetization cycle $M(H)$ and the heat capacity dependence $C_m(T,H)$ within the Boltzmann statistics, at each temperature and applied field. Since $H_{Tb,i}$ can be fully determined from the *ab initio* results, a preliminary modeling of the experimental data was done

Published on 20 March 2019. Downloaded by University of Edinburgh on 3/25/2019 10:48:02 AM.

Dalton Transactions Accepted Manuscript

View Article Online
DOI: 10.1039/C8DT05044A

Published on 20 March 2019. Downloaded by University of Edinburgh on 3/25/2019 10:48:02 AM.

using the magnetic coupling constant J' as the only adjustable parameter. This approach provided a qualitative agreement for the susceptibility and magnetization, but failed to fit the heat capacity, with calculated peaks of the $C_m(T,H)$ curves at lower temperatures than the experimental ones. Low temperature heat capacity is very sensitive to Δ_{Tb}, therefore, taking into account that the CASPT2/RASSI-SO method can produce an error of a few Kelvin in the determination of energy levels, in our second approach Δ_{Tb} was also treated as a free parameter, but keeping unaltered all the other single-ion energy levels and the single-ion eigenstates from the *ab initio* calculation. Then, the final modelization of the experimental data was performed iteratively, leaving both J' and Δ_{Tb} as adjustable parameters, until finding a set of parameters fitting, simultaneously, $M(H)$, $\chi(T)$ and $C_m(T,H)$. It is worth noting that, whereas J' and Δ_{Tb} were highly correlated in the fitting of the $M(H)$, $\chi(T)$ data, the heat capacity peaks' position was mainly determined by Δ_{Tb} allowing an unequivocal determination of the parameters. The hyperfine constant was settled by the fitting of the HC at low temperatures and high fields. The calculated equilibrium thermodynamic functions for the best fit parameters, $\Delta_{Tb}/k_B = 3.22$ K, $J'/k_B = -0.011$ K and A=25 mK ($J'^*/k_B = -1.6$ K and A*=0.3 K expressed in a S*=1/2 Hamiltonian, Eq. [S4]), and their comparison with the experimental curves, are shown in the next experimental sections.

5. Static results

Susceptibility

Figure 4 shows the temperature dependence of the susceptibility measured by SQUID in the 300-1.8 K range. The χT product at room temperature approaches the expected value of $\chi T_{t,free} = 2\, g_J^2 J(J+1)/8$ = 23.6 emu.K/mol for two free Tb(III) ions ($^7F_6$, S = 3, L = 3, J = 6, g_J = 3/2), and yields an experimental effective moment of μ_{eff} = 9.71 μ_B.

Additional ac susceptibility measurements at very low frequency (f = 40 Hz) performed in a dilution refrigerator allowed us obtaining the $\chi'(T)$ curve down to T=50 mK. The experimental data were scaled to absolute values measured by SQUID in the range 1.8 K to 3 K in order to account for geometrical effects which differ between the two instruments[49]. A maximum in the $\chi'(T)$ curve appears at T_{max}= 0.09 K. The χT product decreases monotonically with decreasing temperature due to thermal depopulation of crystal field splitted levels. The observed decrease below room temperature, down to 2 K, is correctly fitted by the dimer Hamiltonian in Eq. [4] with a single-ion $\Delta_{Tb}/k_B = 3.22$ K and an intradimer coupling constant of $J'^*/k_B = -1.6$ K (in the S*=1/2 Hamiltonian), see Fig. 4. This interaction is mainly of dipolar origin, given its proximity to the calculated intradimer dipolar interaction, $J^{'*}_{dip}/k_B = -1.02$ K (Table 2).

Below 2 K, the theoretical dimeric model predicts lower values for the χT product than observed in the experiment. Indeed, the effective magnetic moment derived from measurements at the lowest temperature, 50 mK, yields μ_{eff} = 2.23 μ_B per Tb dimer to be compared with μ_{eff} = 1.85 μ_B predicted with the dimer model. This discrepancy is more obvious in the $\chi'(T)$ data (see inset Fig. 4), where the equilibrium prediction including hyperfine interaction falls below experimental values. This extra contribution cannot be explained in terms of the susceptibility of two Tb(III) ions with non-parallel EAM axes, as has been done in another dimeric Tb_2 complex reported by F. Luis *et al.*[18], since in our case the EAM axes of the two

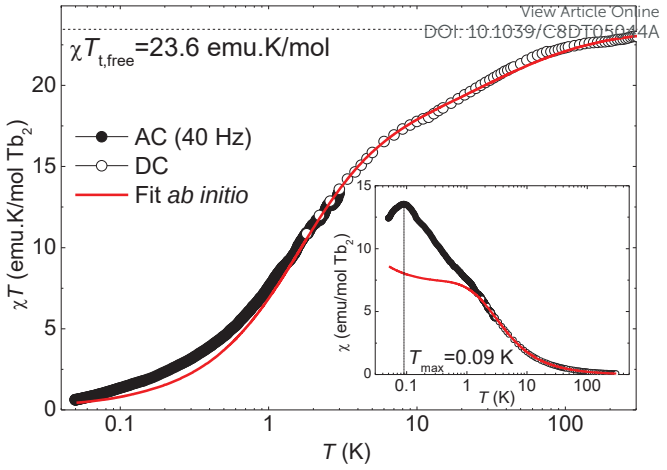

Fig. 4 Susceptibility-temperature product (χT) measured by SQUID in DC (open symbols), and in the Dilution Refrigerator in AC at very low frequency, f=40 Hz (bold symbols); Dashed line: $\chi T_{t,free}$ limit for two non-interacting ions; Red line: fit within the Hamiltonian model for the Tb_2 dimer with the single-ion $\Delta_{Tb}/k_B = 3.22$ K, intradimer interaction $J'/k_B = -0.011$ K ($J'^*/k_B = -1.6$ K) and hyperfine dipolar constant A=25 mK (A*=0.3 K). (Inset): susceptibility as a function of the temperature.

Tb(III) ions are exactly antiparallel because they are related by an inversion centre.

The dimer model considered, predicts a $\chi(T)$ plateau stemming from the population of the electronic ground state singlet (the hyperfine contribution, small compared to the electronic one, only produces a small uprise at very low temperatures). The absence of this plateau, and additional susceptibility contribution present below 2 K indicates that there are other interactions outside the dimer model generating lower energy level splitting. A plausible origin of these energy level splittings could be related with the existence of a large number of dipolar interactions between each Tb(III) ion and their neighbor ions outside the dimer (for instance there are 21 neighbor Tb ions below the distance of 15 Å) which are not taken into account in the dimer model. From the concavity of the energy of the dimer ground state as a function of the magnetic field at H=0 (see Figure 3b), it is inferred that moving the dimer ground state out of the local maximum becomes energetically favorable. Therefore, the crystal short-range magnetic configurations in which the Tb ions have small magnetic moments (producing a dipolar magnetic field which, in turn, induces the previous magnetic moments in a self-consistent way), could have a lower enthalpy than the crystal magnetic configuration in which all the magnetic moments are quenched and there is not an induced dipolar magnetic field. With this respect, the presence of numerous defects[35] in the polymeric chain could enhance both the induced magnetic moments and their associated dipolar magnetic field by modifying the crystal environment and by suppressing the dimer magnetic interaction. Fig. S3 shows how the presence of single-ion moments increases the $\chi(T)$ susceptibility. Unluckily, the large complexity of computational simulation for such a 3D-dimensional system with a large number of dipolar interactions makes it unaffordable.

Dalton Transactions Accepted Manuscript

 This journal is © The Royal Society of Chemistry 20xx

View Article Online
DOI: 10.1039/C8DT05044A

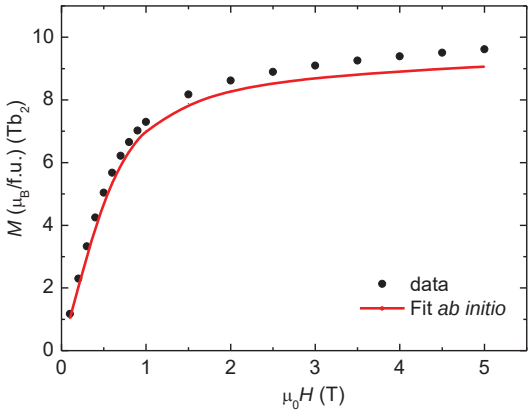

Fig. 5 Field-dependence of the magnetization per formula unit (containing two Tb ions), $M(H)$, measured at T=1.8 K. Line: fit within a dimer model of Tb_2 ions with *ab initio* calculated single-ion $\Delta_{Tb}/k_B = 3.22$ K, and intradimer interaction $J'^*/k_B = -1.6$ K (in the S^*=1/2 Hamiltonian).

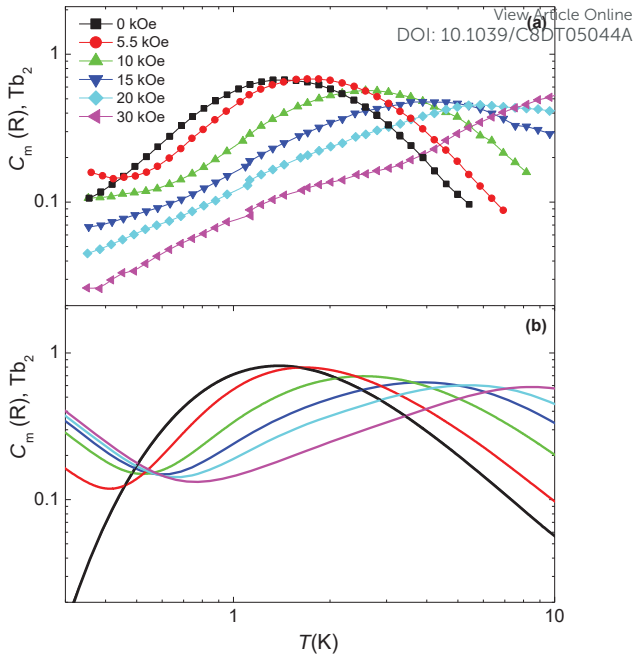

Fig. 6 (a) Magnetic heat capacity data (per Tb_2 dimer) as a function of the temperature at different magnetic fields; (b) Simulations of the HC, using the parameters for the single-ion $\Delta_{Tb}/k_B = 3.22$ K, intradimer interaction $J'^*/k_B = -1.6$ K and hyperfine interaction A^*=0.3 K (in S^*=1/2 Hamiltonian).

Magnetization

The measured $M(H)$ curve at T=1.8 K is shown in Fig. 5, together with the calculated one using the dimer Hamiltonian model, with a single-ion $\Delta_{Tb}/k_B = 3.22$ K, and an intradimer interaction $J'^*/k_B = -1.6$ K. The calculated curve is lower than the experiment, in particular at high magnetic fields. This can be related with the accuracy in the *ab initio* determination of the wavefunctions of the two lowest states, where a higher admixture of J_z eigenstates would produce a larger magnetization when the magnetic field has a component perpendicular to the EAM axis. However, the difference between the model and the experiment may be also due to the dimer model not taking into account the effect of the dipolar interactions, as mentioned above. In this case, the applied magnetic field along the EAM axis will induce magnetic moments on both the Tb ion and the Tb dimer (as can be inferred looking at the slope of the energy levels in Figure 3b) enhancing the magnetic dipolar interactions among the Tb ions and, consequently, also enhancing the induced dipolar magnetic field, which, in turn, will favor a higher magnetization for a given applied magnetic field.

Heat capacity

The temperature dependence of the heat capacity (HC) between 0.3 K and 45 K under different magnetic fields was measured using a commercial Physical Properties Measurement System (PPMS). Figure 6a shows the magnetic heat capacity curves, $C_m(T, H)$, after subtracting the lattice contribution C_{LT}. At H=0, C_m shows a Schottky-type broad anomaly centered at T_{Sc}=1.8 K.

As shown in Figure 6b, the evolution of the experimental curves for increasing applied fields above 1 K is also qualitatively explained under the dimer model. At lower temperatures, a minimum and an upturn in the HC curves appears (clearly observed e.g. in the 5 kOe curve), caused by the the electron-nuclear hyperfine interaction. The data are well reproduced by the dimer model including the hyperfine contribution, Eq. [4], with g_z^*=17.54, g_N=1.342 and A^*=0.3 K. This dipolar hyperfine constant is in good agreement with values previously reported[50, 35].

6. Dynamic results

Zero-field

The ac susceptibility of $\{Tb_2Ba(\alpha\text{-fur})_8\}$ measured within the SQUID temperature range (1.8 K-15 K) showed no frequency dependence. Given that most of the related Ln-furoate complexes exhibit slow relaxation phenomenology at sub-Kelvin temperatures, we decided to conduct further ac measurements down to lower temperatures (50 mK) in a susceptometer installed in a dilution refrigerator at Quantum Design[44]. The data are shown in Fig. 7, once they have been scaled to the $\chi'(T)$ SQUID data.

It can be observed that both $\chi'(T)$ and $\chi''(T)$ present maxima, even at the lowest frequency (40 Hz). The $\chi'(T)$ and $\chi''(T)$ peaks decrease in intensity and are shifted to higher temperatures for increasing f. From the frequency-shift of the $\chi''(T)$ peak, the relaxation time as a function of the reciprocal temperature, $\tau(1/T)$, has been deduced, Figure 8c. The relaxation process follows an Orbach-type temperature dependence, with an activation energy U/k_B=1.1 K and τ_0=1.72x10^{-10} s.

From the static behavior we have concluded that the excess in χ' has its origin in a 3D-short range ordering of induced magnetic moments promoted by inter-dimer and interchain dipolar interactions and probably enhanced by numerous defects[35] in the polymeric chains. Moreover, these defects would give rise to uncompensation in the induced magnetic moments, which in turn cause magnetic disorder in the 3D-lattice. The relaxation process detected is probably caused by the sluggish response of the small induced magnetic moments to the ac excitation.

Published on 20 March 2019. Downloaded by University of Edinburgh on 3/25/2019 10:48:02 AM.

Dalton Transactions Accepted Manuscript

View Article Online
DOI: 10.1039/C8DT05044A

Published on 20 March 2019. Downloaded by University of Edinburgh on 3/25/2019 10:48:02 AM.

Non-zero field

The study of the relaxation behavior under applied magnetic fields was conducted in a SQUID susceptometer. The χ', $\chi''(f, H)$ curves recorded at T=2.0 K as a function of the applied field, and χ', $\chi''(f, T)$ data at H=4.5 kOe (the optimum field at which the intensity of the $\chi''(f,H,2K)$ peak was maximum), are shown in Fig. 8a and Fig. 8b, respectively.

A clear slow relaxation process with high intensity χ'' peak is observed at low frequencies, while another, of very much smaller intensity is hinted at higher frequency. The presence of the two relaxation processes is more clearly evidenced in the $\chi''(\chi')$ Cole-Cole plot representation, as shown in Fig. S4. The dependence of the relaxation times for the two processes, τ_{lf} and τ_{hf}, as a function of the inverse temperature, $\tau(1/T)$, and the field, $\tau(H)$, have been derived from the position of the χ'' peaks and are shown in Fig. 8c and 8d, respectively. Notice that the main relaxation mechanism is a very slow process ($\tau \approx 0.3$ s), and its H dependence is very weak.

It is quite similar to very slow processes previously found in all Ln polymeric chains we have studied[32,38,35]. The field induced slow relaxation has no relation with the relaxation process detected at H=0. In fact, at $H \neq 0$ it is caused by a direct process affected by strong bottleneck (BE) effect since in the SQUID experiment the thermal contact with the bath through He exchange gas is poor compared with the DR case.

To demonstrate the strong influence of the BE in our system, we performed $\chi''(f)$ measurements in the SQUID susceptometer under different gas pressures. As demonstrated in Fig. 9, when the chamber is vented, instead of purged, there is an increase in the thermal contact between the sample and the bath, which increases by two orders of magnitude the relaxation rate. By settling back the chamber conditions the relaxation rate decreases reversibly. Therefore, no intrinsic magnetic information on the spin relaxation rate can be extracted.

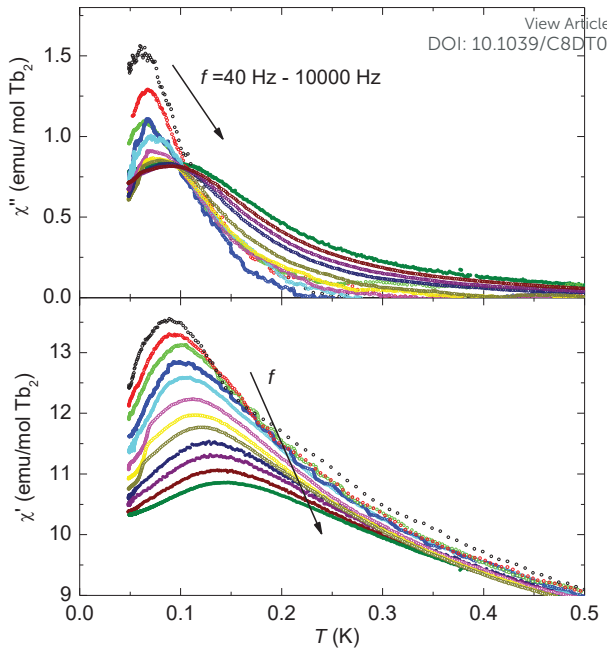

Fig. 7 Out-of-phase $\chi''(T)$ and in-phase $\chi'(T)$ ac susceptibility of T measured at H=0 and different frequencies, down to 50 mK.

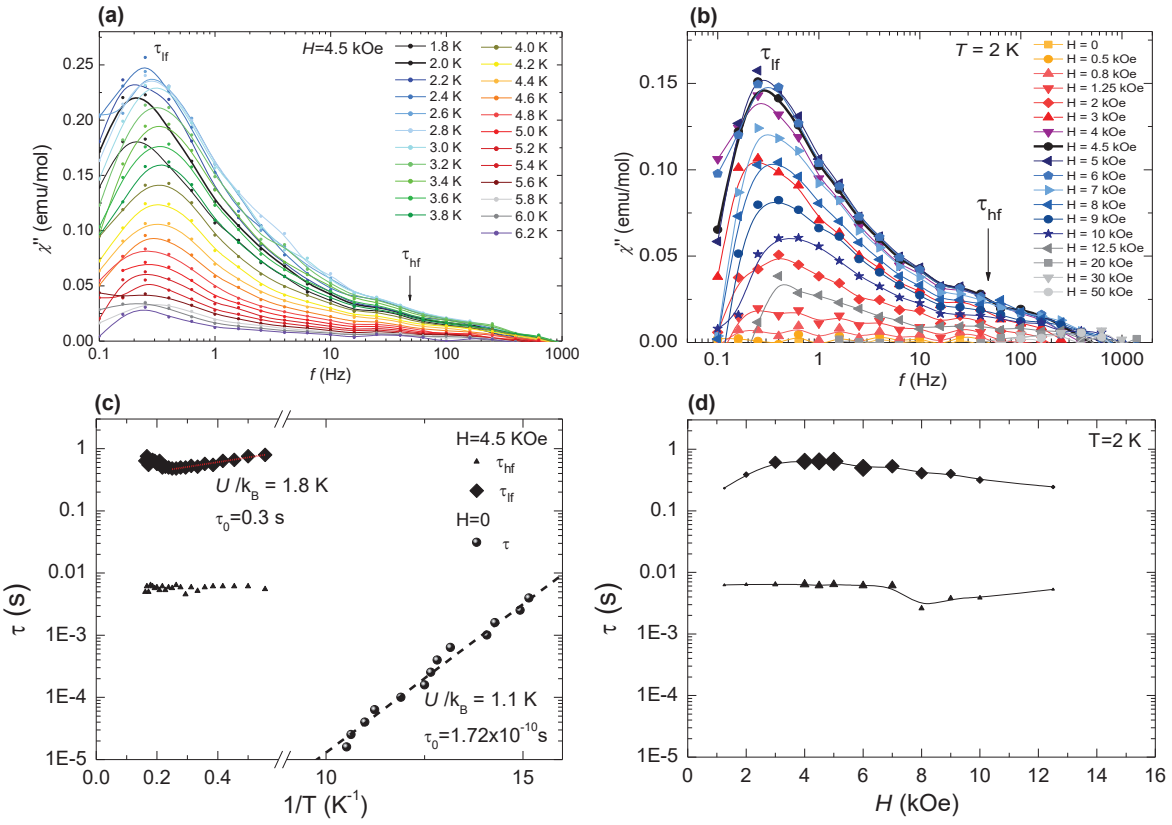

Fig. 8 Top: AC susceptibility results measured by SQUID results in $H \neq 0$: (a) $\chi''(f)$ at constant H=4.5 kOe, at different temperatures, (b) $\chi''(f)$ at different magnetic fields, at T=2.0 K. Bottom: (c) Relaxation time *vs.* inverse of the temperature, at H=0, and H=4.5 kOe, where two different relaxation processes can be observed; (d) relaxation time as a function of the applied field, at constant T=2.0 K.

Dalton Transactions Accepted Manuscript

This journal is © The Royal Society of Chemistry 20xx

View Article Online
DOI: 10.1039/C9DT00510F

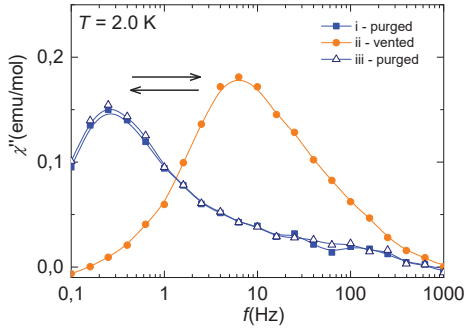

Fig. 9. $\chi''(f)$ at T=2 K, H=4.5 kOe measured in the SQUID susceptometer under different pressure conditions: experiments were performed with the chamber i) purged or ii) vented; the $\chi''(f)$ curve is recovered one the chamber is purged again (iii).

Discussion

In this section we discuss, with the help of Figure 10, the magnetic behavior of **(Tb$_2$Ba)** complex compared with that of the previously studied α-furoates: the **(Dy$_2$Ba)**[38], and monomeric **(Dy)**[32], **(Tb)**[35] complexes.

The magnetic structure of **(Dy)**[32] is formed by two different types of linear chains (including either Dy(A) or Dy(B) sites) having an uncompensated ferromagnetic spin-canted intrachain coupling (J_c*/k_B = 0.755 K). The two Dy sites, which differ only in the position of one of the capping ligands, show SIM relaxation through Thermally Activated Quantum Tunneling (TAQT) with different activation energies, 80.5 K and 32.4 K, respectively, until reaching a quantum tunneling (QT) regime upon cooling. As the temperature is decreased, weak interchain AF coupling (J_{ab}*/k_B= -0.135 K), of dipolar origin, allows the establishment of an AF 3D long-range ordering at T_N = 0.66 K.

In the compound **(Dy$_2$Ba)** the α-furoates consolidate 1D zig-zag chains formed by Dy_2 separated by Ba ions, like in isostructural Tb_2Ba. However, as shown by *ab initio*, for the same distorted SAP coordination environment, the EAM in the Ln=Dy complex is deviated from the quasi-C_4 axis by 44º, while for the Ln=Tb counterpart the EAM is practically perpendicular to C_4. Hence while in the **(Dy$_2$Ba)** complex the EAM of the Dy ions are slightly canted with respect to the c-axis chain direction and intrachain interactions are Ferromagnetic (FM), for the **(Tb$_2$Ba)** complex the EAM are nearly orthogonal to the chain axis, and intrachain Tb coupling is AF. In the **(Dy$_2$Ba)** complex magnetic dimerization does not play a significant role (intradimer and interdimer interactions are of the same order), and thus the magnetic properties of the chain can be described by an average, intrachain coupling constant J*. In contrast, the Tb-Tb intradimer AF interaction in **(Tb$_2$Ba)** is relevant since it is of the order of the anisotropy energy, while the interdimer interaction is an order of magnitude smaller.

Regarding the spin dynamics, when approaching T=0 the phenomenology of **(Dy$_2$Ba)** is similar to that observed for **(Dy)**: under H=0, relaxation proceeds through QTM of the Dy ions, until reaching at T_N = 0.25 K a long-range 3D ordering state enabled by the AF interchain coupling (J'''/k_B = -0.021 K). The smaller T_N and more pronounced critical slowing down of the tunneling rate observed for **(Dy$_2$Ba)** than for **(Dy)** could be well rationalized in terms of the calculated magnitudes of the dipolar field $\sigma_{dip,xy}$ and the dipolar intrachain interactions[38]. The application of a magnetic field opens up the path for slow relaxation of the Dy ions through an Orbach process (U/k_B = 68 K at H=2 kOe); in addition, a second slower process with τ~0.2 s is observed.

The dynamical behavior of **(Tb$_2$Ba)**, in contrast, qualitatively resembles that of **(Tb)**. In the latter, two slightly different coordination sites, Tb(A) and Tb(B), are distinguished, depending on the relative positions of a water and a dangling α-furoate with respect to the distorted trigonal bipiramidal polyhedron. This gives rise to the existence of two different types of chains (A and B) in the crystal. At any rate, in both of them, and similar to **(Tb$_2$Ba)**, the EAM of Tb ions are nearly perpendicular to the chain, and intrachain coupling is AF (J*/k_B~-0.135 K). In H=0 two Arrhenius-like processes are observed, with activation energies 2.03 K and 1 K, associated to SCM relaxation in the two types of chains, enabled by the presence of defects breaking the chain in shorter segments. In such an AF chain, 3D ordering can never be achieved when approaching T→0, unlike in **(Dy$_2$Ba)**. It is found instead that for T<0.1 K the SCM mechanism is replaced by individual relaxation of the ions through direct processes. For **(Tb$_2$Ba)** under H=0 slow relaxation is assigned to sluggish relaxation of the remaining magnetic moments, possibly enhanced by the presence of defects in the dimeric chain. The observed activation energy (U/k_B=1.1 K) in **(Tb$_2$Ba)** is similar to that of **(Tb)**, something which is explained by the fact that the magnitudes of Δ_{2Tb} and interdimer interaction J''^* of the former are similar to Δ_{Tb} and J'* in the mononuclear compound. Under the application of a magnetic field, both for **(Tb$_2$Ba)** and **(Tb)** two different direct, bottlenecked slow relaxation process are observed. The $\tau(1/T)$ and $\tau(H)$ (shown in Fig. S5) dependencies of these processes in the two compounds are remarkably similar.

Conclusions

In summary, a new one-dimensional magnet of the α-furoate family, $\{Tb_2Ba(\alpha\text{-fur})_8\}_n$, has been fully characterised. From the magnetic point of view, above 2 K the complex can be modeled as a system of non-Kramers Tb ions with $\Delta_{Tb}/k_B = 3.22$ K, coupled in antiferromagnetic dimers with an AF interaction $J'^*/k_B = -1.6$ K, and weakly connected in chains by interdimeric interaction, and between chains by interchain dipolar interaction. Below 2 K, defects cause uncompensation of the magnetic moments, which create magnetic disorder in the 3D lattice. The sluggish response of the disordered spin system gives rise to the relaxation process, with activation energy U/k_B=1.1 K. Field-induced slow relaxation occurs through two different, bottlenecked direct processes. Above 2 K the effects of dimerization in this complex are negligible, and thus the dynamic magnetic behavior is qualitatively very similar to that of the monomeric complex $\{Tb(\alpha\text{-fur})_3\}$ previously reported. In contrast, the replacement of Dy by Tb in $\{Ln_2Ba(\alpha\text{-fur})_8\}$ leads to profound consequences on the relaxational phenomena. The present work constitutes a rare example of a polimeric system of AF coupled dimers of non-Kramers ions displaying slow relaxation dynamics.

Acknowledgements

This work has been financed by MECOM Projects MAT2014-53921-R, MAT2015-68200-C02-2-P and MAT2017-83468-R. We are grateful to Javier Rubín for his critical reading of the manuscript. D. P. thanks the Alexander von Humboldt (AvH) Foundation for financial support.

Published on 20 March 2019. Downloaded by University of Edinburgh on 3/25/2019 10:48:02 AM.
Dalton Transactions Accepted Manuscript

View Article Online
DOI: 10.1039/C8DT05044A

Published on 20 March 2019. Downloaded by University of Edinburgh on 3/25/2019 10:48:02 AM.

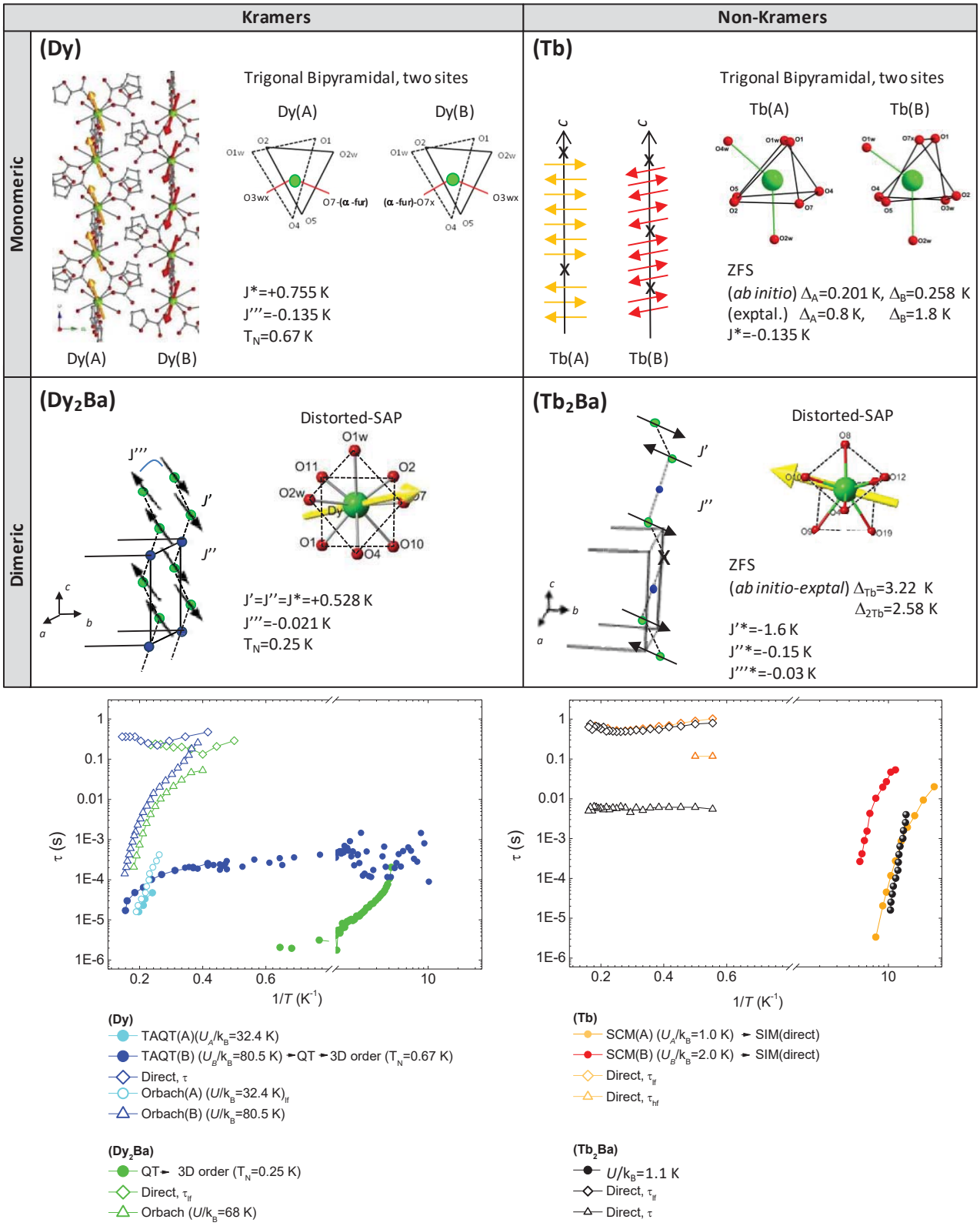

Fig. 10 Comparison of magneto-structural properties of the Ln α-furoate complexes: magnetically monomeric **(Dy)**[32], **(Tb)**[35] and dimeric **(Dy_2Ba)**[38] and **(Tb_2Ba)** (this work); (Bottom) Summary of relaxation processes.

Dalton Transactions Accepted Manuscript

This journal is © The Royal Society of Chemistry 20xx

View Article Online
DOI: 10.1039/C8DT05048A

References

1 R. A. Layfield and M. Murugesu, *Lanthanides and Actinides in Molecular Magnetism*, Wiley-VCH Verlag&Co. KGaA, 2015.

2 E. Bartolomé, A. Arauzo, J. Luzón, J. Bartolomé and F. Bartolomé, in *Handbook of Magnetic Materials*, ed. E. Brück, Elsevier, 2017, pp. 1–289.

3 C. A. P. Goodwin, F. Ortu, D. Reta, N. F. Chilton and D. P. Mills, *Nature*, 2017, **548**, 439–442.

4 J. Rinehart and J. Long, *Chem. Sci.*, 2011, **2**, 2078–2085.

5 J. Jung, T. T. da Cunha, B. Le Guennic, F. Pointillart, C. L. M. Pereira, J. Luzon, S. Golhen, O. Cador, O. Maury and L. Ouahab, *Eur. J. Inorg. Chem.*, 2014, 3888–3894.

6 L. Ungur, J. J. Leroy, I. Korobkov, M. Murugesu and L. F. Chibotaru, *Angew. Chemie - Int. Ed.*, 2014, **53**, 4413–4417.

7 J. Liu, Y. C. Chen, J. L. Liu, V. Vieru, L. Ungur, J. H. Jia, L. F. Chibotaru, Y. Lan, W. Wernsdorfer, S. Gao, X. M. Chen and M. L. Tong, *J. Am. Chem. Soc.*, 2016, **138**, 5441–5450.

8 L. Ungur, M. Thewissen, J. P. Costes, W. Wernsdorfer and L. F. Chibotaru, *Inorg. Chem.*, 2013, **52**, 6328–6337.

9 G. Gupta and G. Rajaraman, *J. Chem. Sci.*, 2014, **126**, 1569–1579.

10 V. E. Campbell, H. Bolvin, E. Rivière, R. Guillot, W. Wernsdorfer and T. Mallah, *Inorg. Chem.*, 2014, **53**, 2598–2605.

11 K. S. Pedersen, L. Ungur, M. Sigrist, A. Sundt, M. Schau-Magnussen, V. Vieru, H. Mutka, S. Rols, H. Weihe, O. Waldmann, L. F. Chibotaru, J. Bendix and J. Dreiser, *Chem. Sci.*, 2014, **5**, 1650–1660.

12 F. S. Guo, B. M. Day, Y. C. Chen, M. L. Tong, A. Mansikkamäki and R. A. Layfield, *Angew. Chem. Int. Ed.*, 2017, **56**, 11445–11449.

13 F.-S. Guo, B. M. Day, Y.-C. Chen, M.-L. Tong, A. Mansikkamäki and R. A. Layfield, *Science (80-.).*, 2018, **364**, 1400–1403.

14 Y. N. Guo, G. F. Xu, W. Wernsdorfer, L. Ungur, Y. Guo, J. Tang, H. J. Zhang, L. F. Chibotaru and A. K. Powell, *J. Am. Chem. Soc.*, 2011, **133**, 11948–11951.

15 C. Y. Chow, H. Bolvin, V. E. Campbell, R. Guillot, J. F. Kampf, W. Wernsdorfer, F. V Gendron, J. Autschbach, V. L. Pecoraro and T. Mallah, *Chem. Sci.*, 2015, **6**, 4148–4159.

16 F. Cimpoesu,, Dahan F, S. Ladeira, M. Ferbinteanu and J. P. Costes, *Inorg.Chem.*, 2012, **51**, 11279–11293.

17 A. Baniodeh, Y. Lan, G. Novitchi, V. Mereacre, A. Sukhanov, M. Ferbinteanu, V. Voronkova, A. C.E. and A. K. Powell, *Dalt. Trans.*, 2013, **42**, 8926–8938.

18 F. Luis, A. Repollés, M. J. Martínez-Pérez, D. Aguilá, O. Roubeau, D. Zueco, P. J. Alonso, M. Evangelisti, A. Camón, J. Sesé, L. A. Barrios and G. Aromí, *Phys. Rev. Lett.*, 2011, **107**, 117203–117208.

19 D. Aguilà, L. A. Barrios, V. Velasco, O. Roubeau, A. Repollés, P. J. Alonso, J. Sesé, S. J. Teat, F. Luis and G. Aromí, *J. Am. Chem. Soc.*, 2014, **136**, 14215–14222.

20 E. Moreno-Pineda, S. Klyatskaya, P. Du, Damjanovic, G. Taran, W. Wernsdorfer and M. Ruben, *Inorg. Chem.*, 2018, **57**, 9873–9879.

21 R. J. Holmberg, M. A. Polovkova, A. G. Martynov, Y. G. Gorbunova and M. Murugesu, *Dalton Trans.*, 2016, **45**, 9320–9327.

22 T. Morita, M. Damjanović, K. Katoh, Y. Kitagawa, N. Yasuda, Y. Lan, W. Wernsdorfer, B. K. Breedlove, M. Enders and M. Yamashita, *J. Am. Chem. Soc.*, 2018, **140**, 2995–3007.

23 R. J. Holmberg, I. Korobkov and M. Murugesu, *RSC Adv.*, 2016, **6**, 72510–72518.

24 A. V. Gavrikov, P. S. Koroteev, Z. . Dobrokhotova, A. B. Ilyukhin, N. N. Efimova, D. I. Kirdyankin, M. A. Bykovb, M. A. Ryumina and V. M. Novotortsev, *Polyhedron*, 2015, **102**, 48–59.

25 P. I. Girginova, L. C. J. Pereira, J. T. Coutinho, I. C. Santos and M. Almeida, *Dalton Trans.*, 2014, **43**, 1897–905.

26 Y. Li, J. W. Yu, Z. Y. Liu, E. C. Yang and X. J. Zhao, *Inorg. Chem.*, 2015, **54**, 153–160.

27 A. B. Castro, J. Jung, S. Golhen, B. Le Guennic, L. Ouahab, O. Cador and F. Pointillart, *Magnetochemistry*, 2016, **2**, 1–11.

28 M. Yatoo, G. Cosquer, M. Morimoto, M. Irie, B. Breedlove and M. Yamashita, *Magnetochemistry*, 2016, **2**, 1–8.

29 G. Cosquer, F. Pointillart, J. Jung, B. Le Guennic, S. Golhen, O. Cador, Y. Guyot, A. Brenier, O. Maury and L. Ouahab, *Eur. J. Inorg. Chem.*, 2014, **2014**, 69–82.

30 W.-H. Zhu, Y. Zhang, Z. Guo, S. Wang, J. Wang, Y.-L. Huang, L. Liu, Y.-Q. Fan, F. Cao and S.-W. Xiang, *RSC Adv.*, 2014, **4**, 49934–49941.

31 A. K. Mondal, H. S. Jena, A. Malviya and S. Konar, *Inorg. Chem.*, 2016, **55**, 5237–5244.

32 E. Bartolomé, J. Bartolomé, S. Melnic, D. Prodius, S. Shova, A. Arauzo, J. Luzón, F. Luis and C. Turta, *Dalton Trans.*, 2013, **42**, 10153–10171.

33 R. Sessoli and K. Bernot, in *Lanthanides and actinides in molecular magnetism,* eds. R. Layfield and M. Murugesu, Wiley-VCH, 2015, pp. 89–123.

34 W.-X. Zhang, R. Ishikawa, B. Breedlove and M. Yamashita, *RSC Adv.*, 2013, **3**, 3772–3798.

35 E. Bartolomé, J. Bartolomé, A. Arauzo, J. Luzón, L. Badía, R. Cases, F. Luis, S. Melnic, D. Prodius, S. Shova and C. Turta, *J. Mater. Chem. C*, 2016, **4**, 5038–5050.

36 Y. Wang, X. L. Li, Y. Song and X. Z. You, *Inorg. Chem.*, 2010, **49**, 969–976.

37 C. Turta, S. Melnic, M. Bettinelli, S. Shova, C. Benelli, A. Speghini, A. Caneschi, M. Gdaniec, Y. Simonov, D. Prodius and V. Mereacre, *Inorg. Chim. Acta*, 2007, **360**, 3047–3054.

38 E. Bartolomé, J. Bartolomé, S. Melnic, D. Prodius, S. Shova, A. Arauzo, J. Luzón, L. Badía-Romano, F. Luis and C. Turta, *Dalton Trans.*, 2014, **43**, 10999–11013.

39 E. Bartolomé, J. Bartolomé, A. Arauzo, J. Luzón, R. Cases, S. Fuertes, V. Sicilia, A. I. Sánchez-Cano, J. Aporta, S. Melnic, D. Prodius and S. Shova, *J. Mat. Chem. C*, 2018, **6**, 5286–5299.

40 S. Melnic, D. Prodius, S. Shova, H. Stoeckli-Evans, Y. Simonov, A. Feher, M. Gdaniec and C. Turta, *Chem. J. Mold.*, 2009, **4**, 61–69.

41 *CrysAlis RED, Oxford Diffr. Ltd., Version 1.171.34.76*.

42 O. V. Dolomanov, L. J. Bourhis, R. J. Gildea, J. A. K. Howard and H. Puschmann, *J. Appl. Crystallogr.*, 2009, **42**, 339–341.

43 G. M. Sheldrick, *Acta Cryst.*, 2008, **A64**, 112–122.

44 A. Andreas, N. Manivannan, M. Luis, W. Alan and S. Stefano, *IEEE Trans. Appl. Supercond.*, 2017, **27**, 1–4.

45 B. . Roos and P. A. Malmquist, *Phys. Chem. Chem. Phys.*, 2004, **6**, 2919–2937.

46 F. Aquilante, L. de Vico, N. Ferré, G. Ghigo, P.-Å. Malmqvist, P. Neogrády, T. Pedersen, M. Pitonák, M. Reiher, B. O. Roos, L. Serrano-Andrés, M. Urban, V. Verzayov and R. Lindh, *J. Comput. Chem.*, 2010, **31**, 224–247.

47 G. Cucinotta, M. Perfetti, J. Luzon, M. Etienne, P. E. Car, A. Caneschi, G. Calvez, K. Bernot and R. Sessoli, *Angew. Chemie*

Published on 20 March 2019. Downloaded by University of Edinburgh on 3/25/2019 10:48:02 AM.

Dalton Transactions Accepted Manuscript

View Article Online
DOI: 10.1039/C8DT05044A

- *Int. Ed.*, 2012, **51**, 1606–1610.
48 J. S. Griffith, *Phys. Rev.*, 1963, **132**, 316–319.
49 *Quantum Design Application Note 1091-217, available online*, 2018.
50 N. Ishikawa, M. Sugita and W. Wernsdorfer, *Angew. Chemie - Int. Ed.*, 2005, **44**, 2931–2935.

Published on 20 March 2019. Downloaded by University of Edinburgh on 3/25/2019 10:48:02 AM.

Dalton Transactions Accepted Manuscript

This journal is © The Royal Society of Chemistry 20xx

Published on 20 March 2019. Downloaded by University of Edinburgh on

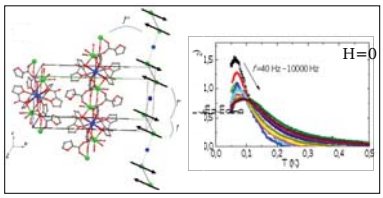

The new polymeric magnet $\{[Tb_2Ba(\alpha\text{-fur})_8(H_2O)_4]\cdot 2H_2O\}_n$ constitutes a rare example of AF coupled dimers of non-Kramers ions displaying slow relaxation dynamics.

Dalton Transactions Accepted Manuscript